

Impact of the radial profile of atomic nuclei on observables in high-energy collisions

Zhengxi Yan,^{1,*} Jun Xu,^{2,†} and Jiangyong Jia^{1,3,‡}

¹*Department of Chemistry, Stony Brook University, Stony Brook, NY 11794, USA*

²*School of Physics Science and Engineering, Tongji University, Shanghai 200092, China*

³*Physics Department, Brookhaven National Laboratory, Upton, NY 11976, USA*

In heavy-ion phenomenology, the nucleon density distribution in colliding nuclei is commonly described by a two-parameter Woods-Saxon (WS) distribution. However, this approach omits the detailed radial structure in the density distribution that arise from quantal filling patterns of neutrons and protons. These fine structures, as estimated by the Skyrme-Hartree-Fock density functional, cause small deviations in heavy-ion observables from the WS baseline, which cannot be captured by simply readjusting the WS parameters. These deviations are dependent on centrality and observable but often exhibit similar shapes for different nuclei. Such fine structures may introduce up to a 25% uncertainty in the measured differences in heavy-ion observables between the $^{96}\text{Ru}+^{96}\text{Ru}$ and $^{96}\text{Zr}+^{96}\text{Zr}$ mid-central collisions from the STAR Collaboration.

High-energy nuclear collisions at RHIC and LHC generate a hot and dense quark-gluon plasma (QGP), whose space-time expansion is governed by relativistic viscous hydrodynamic equations [1]. These collisions, due to their extremely short timescales, effectively capture a snapshot of the nucleon spatial distribution in the nuclei, forming the initial condition of the QGP. This initial condition, through hydrodynamic expansion, imprints patterns on the particle momentum distributions observed in detectors [2]. Although this high-energy imaging concept is theoretically powerful, it was previously deemed impractical for determining nuclear structure. However, recent developments show that this can be achieved by comparing nuclei with similar masses but different internal structures [3]. By constructing ratios of bulk observables between collisions of such nuclei, the effects of hydrodynamic response are canceled out, isolating the global shape and size features of the colliding nuclei [4]. For instance, the STAR experiment successfully extracted the shape of ^{238}U [5], matching extractions based on low-energy spectroscopic measurements. Other studies of isobar or isobar-like systems of varying sizes also demonstrate the sensitivity of these ratios to the global characteristics of the nuclei involved [6–11].

In high-energy collisions, nuclear structure influences the geometric features of the QGP's initial condition, such as ellipticity ε_2 , triangularity ε_3 , and the number of participating nucleons N_{part} . These geometric features are linearly related to observables describing collective behavior, like elliptic flow v_2 , triangular flow v_3 , and charged particle multiplicity N_{ch} [12, 13]. Since isobar nuclei share the same mass number, deviations from unity in their ratios must arise from differences in nuclear structure, making them power tools for imaging nuclear structure.

In current high-energy phenomenology, the global structure of nuclei is often parameterized by the deformed

Woods-Saxon (WS) function,

$$\rho(r, \theta, \phi) \propto [1 + \exp(r - R_0(1 + f(\theta, \phi))/a)]^{-1}, \quad (1)$$

where R_0 and a represent the half-density radius and skin thickness, respectively. The function $f(\theta, \phi)$ accounts for nuclear deformations by modulating the nuclear surface. For example, for axial-symmetric quadrupole and octupole deformation, $f(\theta, \phi) = \beta_2 Y_{2,0}(\theta, \phi) + \beta_3 Y_{3,0}(\theta, \phi)$. The ratios of observables between two isobar systems $\mathcal{O} = v_n$ and N_{ch} or ε_n and N_{part} , follow a scaling relation as a function of centrality [14]:

$$R_{\mathcal{O}} \equiv \frac{\mathcal{O}_X}{\mathcal{O}_Y} \approx 1 + c_1 \Delta R_0 + c_2 \Delta a + c_3 \Delta \beta_2^2 + c_4 \Delta \beta_3^2, \quad (2)$$

where $\Delta R_0 = R_{0,X} - R_{0,Y}$, $\Delta a = a_X - a_Y$, and $\Delta \beta_n^2 = \beta_{n,X}^2 - \beta_{n,Y}^2$. Indeed, STAR's measurements in $^{96}\text{Ru}+^{96}\text{Ru}$ and $^{96}\text{Zr}+^{96}\text{Zr}$ isobar collisions [15] align well with this scaling relation in both hydrodynamic and transport models with WS parameterizations [14, 16].

However, there is a catch. The actual distribution of the protons and neutrons in the nucleus is more accurately described by Density Function Theories (DFT) based on effective nuclear forces [17]. WS parameters derived from fitting DFT distributions miss detailed features [18], as DFT distributions often show wiggly structures due to the orbital filling pattern of protons and neutrons. In the presence of nuclear deformation, the skin thickness may vary with the polar angle θ [19]. These fine structures' properties depend on specific DFT models and are assumed to have minimal impact on heavy-ion observables, often being ignored in heavy-ion phenomenology.

This paper aims to quantify the impact of the differences between DFT and WS parameterizations on heavy-ion observables. We consider spherical nuclei for simplicity and three observables: ε_2 , ε_3 , and N_{part} . In this context, the scaling relation simplifies to:

$$R_{\mathcal{O}} \approx 1 + c_1 \Delta R_0 + c_2 \Delta a. \quad (3)$$

We compare the results of several representative nuclei with those obtained from the known differences between ^{96}Ru and ^{96}Zr , $\Delta a = a_{\text{Ru}} - a_{\text{Zr}} = -0.06$ fm and $\Delta R_0 = R_{0,\text{Ru}} - R_{0,\text{Zr}} = 0.07$ fm[14]. We found that the differences between DFT and WS have a smaller impact on heavy-ion observables than Δa but can be comparable to ΔR_0 .

Setup. There are many DFTs with many different forces one could choose from [20, 21]. For this study, we use the standard Skyrme-Hartree-Fock (SHF) model [22]. The SHF model defines the parameters of the Skyrme interaction in terms of ten macroscopic quantities, which have empirical values corresponding to the MSL0 force as in Ref. [22, 23]. We generate spatial distributions of protons and neutrons, summing them to obtain the radial distributions of nucleons $\rho(r)$. The parameters R_0 and a are determined by matching the first and second radial moments of the WS distribution to those of the SHF [18]. The n^{th} moment is defined as,

$$\langle r^n \rangle = \frac{\int r^{2+n} \rho(r) dr}{\int r^2 \rho(r) dr}. \quad (4)$$

We scanned a wide range of near spherical nuclei and compared their SHF distributions with the WS fit. From this comparison, we identified three nuclei with characteristically different shapes in $\rho(r)$: ^{96}Zr , ^{112}Sn and ^{197}Au , as shown in Fig. 1. The ^{96}Zr has a wiggle with a dip around $r = 0$, while ^{197}Au exhibits a wiggle with a peak around $r = 0$, both showing significant deviations from the WS distributions. In contrast, ^{112}Sn has a relatively uniform distribution with smaller difference from the WS fit. The corresponding WS parameters are listed in Table I.

	^{96}Zr	^{112}Sn	^{197}Au
R_0 (fm)	5.059	5.538	6.610
a (fm)	0.5774	0.5576	0.5552

TABLE I. Woods-Saxon parameters obtained by matching the first and second moments of nuclear distributions to the SHF.

We used a standard Monte-Carlo Glauber model [24] to simulate collisions of ^{96}Zr , ^{112}Sn , and ^{197}Au , assuming a nucleon-nucleon cross-section of 42 mb. Nucleons are modeled with a hard core, maintaining a minimum separation of 0.4 fm. For each species, 100 million minimum bias events were generated, separately for SHF and WS distributions with their 1st and 2nd radial moments matched. To isolate the impact of the wiggle structure, we constructed another $\rho(r)$ distribution by combining SHF at low radii ($r < R_0 - a$) and WS at higher radii ($r > R_0 - a$) while maintaining the mass number, labeled as ρ_{mix} . Additionally, simulations were repeated by adjusting a by -0.06 fm and R_0 by +0.07 fm to model transitions from ^{96}Zr to ^{96}Ru , labeled as ρ_{WSa^-} and ρ_{WSR^+} , respectively. Thus, five separate simulations were performed for each collision species.

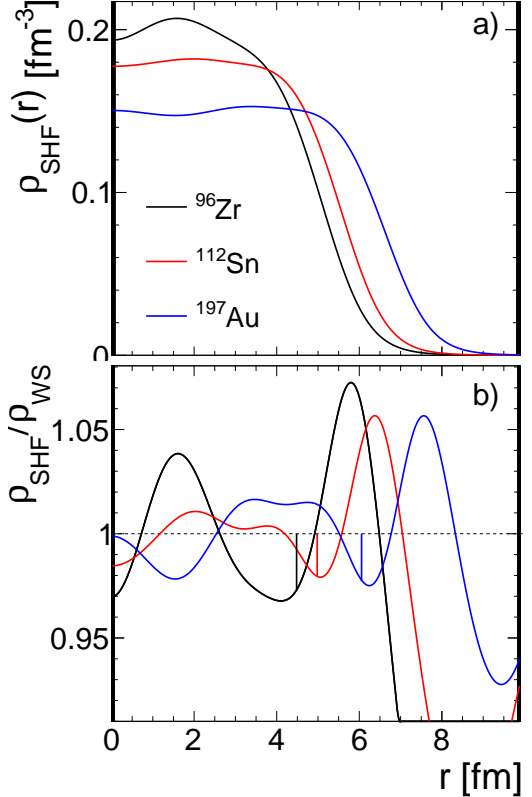


FIG. 1. (a) SHF nucleon density distributions for ^{96}Zr , ^{112}Sn , and ^{197}Au nuclei. (b) Ratio of SHF and WS nucleon density distribution via moment matching. The vertical lines indicate location $r = R_0 - a$, where we combine the SHF to the left and WS to the right together to form ρ_{mix} (see text).

For each event, we calculated N_{part} , ε_2 , and ε_3 , defined from the transverse nucleon density $\rho_{\perp}(r_{\perp}, \phi) = \int \rho dz$ as:

$$\varepsilon_n e^{in\Phi_n} \equiv -\frac{\int \rho_{\perp}(r, \phi) r^n e^{in\phi} r dr d\phi}{\int \rho_{\perp}(r, \phi) r^n r dr d\phi}. \quad (5)$$

We then constructed histograms of $\varepsilon_n \equiv \sqrt{\langle \varepsilon_n^2 \rangle}$ and $p(N_{\text{part}})$ as functions of N_{part} . Note that these wiggly structures still remains in $\rho_{\perp}(r_{\perp})$, but with smaller magnitudes in the inner region (see appendix). The ratios of observables from each distribution were divided by those from the default WS parameterization in Tab. I, resulting in four ratios: $R_{\mathcal{O}}\{\text{SHF}\}$, $R_{\mathcal{O}}\{\text{mix}\}$, $R_{\mathcal{O}}\{\text{WSa}^-\}$, and $R_{\mathcal{O}}\{\text{WSR}^+\}$. These ratios are presented as $R_{\mathcal{O}} - 1$ versus N_{part} .

Results Figure 2 shows the relative differences, $R_{\mathcal{O}}\{\text{SHF}\} - 1$, $R_{\mathcal{O}}\{\text{mix}\} - 1$, $R_{\mathcal{O}}\{\text{WSa}^-\} - 1$, and $R_{\mathcal{O}}\{\text{WSR}^+\} - 1$, as functions of N_{part} for the three observables. In $^{96}\text{A} + ^{96}\text{A}$ collisions, reducing a by 0.06 fm leads to a 2% enhancement in ε_2 in mid-central collisions, while increasing R_0 by 0.07 fm decreases ε_2 by about 0.4%. These behaviors align with the expectation that a more compact source increases ε_2 and vice versa [25]. The impact of both parameters is smaller in peripheral

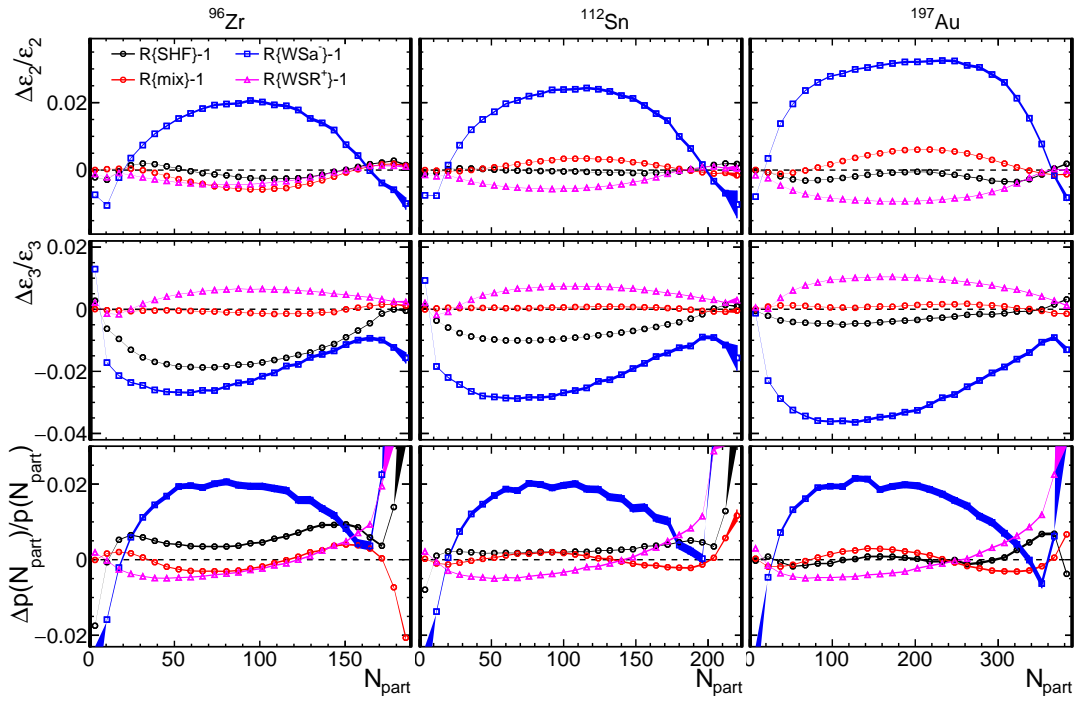


FIG. 2. Glauber model results of $R_O - 1$ for $\mathcal{O} = \varepsilon_2$ (top row), ε_3 (middle row), and $p(N_{\text{part}})$ (bottom row) for Zr+Zr (left column), Sn+Sn (middle column) and Au+Au (right column) collisions. Four ratios are shown: $R_O\{\text{SHF}\} - 1$ (SHF vs. WS), $R_O\{\text{mix}\} - 1$ (Mixed vs. WS), $R_O\{\text{WSa}^-\} - 1$ (WS with a decreased by 0.06 fm vs. without) and $R_O\{\text{WSR}^+\} - 1$ (WS with R_0 increased by 0.07 fm vs. without), see text for explanation.

and central collisions. For larger $^{197}\text{A} + ^{197}\text{A}$ collisions, the impact is more significant: the same variations in a and R_0 lead to a 3.3% increase and a 0.9% decrease in ε_2 , respectively, as larger systems have smaller ε_2 values, amplifying the influence of WS parameter variations. A similar stronger impact is observed for ε_3 (middle row of Fig. 2), with the sign of the relative change opposite to that for ε_2 and occurring at different N_{part} values. These findings are qualitatively consistent with previous studies [6, 26].

The impact on $p(N_{\text{part}})$ can be understood as follows: reducing a sharpens the overlap region's edge, increasing the probability for mid-central and ultra-central events while reducing that in peripheral events, resulting in a broad bump in the ratio, similar to the STAR isobar data [15]. The bump's magnitude is purely geometrical and nearly independent of the system size. In contrast, increasing R_0 slightly reduces $p(N_{\text{part}})$ in mid-central collisions.

The difference between SHF and WS, represented by $R_O\{\text{SHF}\} - 1$, depends on the observable and is shown by open black symbols in Fig. 2, which are more conveniently compared across systems in Fig. 3. Because $\langle r^2 \rangle$ is matched between SHF and WS, the impact on ε_2 , which has an r^2 weight in its definition (Eq.5), is minimal. However, ε_3 from SHF is about 2% smaller than from WS in mid-central collisions, due to the r^3 weight in

ε_3 enhancing contributions from nucleons at the edge of the overlap region. As seen in Fig. 1b, the WS distribution has more contribution from the large r region, where $\rho_{\text{SHF}} < \rho_{\text{WS}}$, significantly affecting mid-central collisions. The impact on $p(N_{\text{part}})$ is small except in ^{96}Zr , where it reaches about 0.4–0.6% in mid-central collisions. The larger outer bump around R_0 in Fig. 1b, more significant in ^{96}Zr , enhances $p(N_{\text{part}})$ in mid-central collisions. The overall shape of $R_O\{\text{SHF}\} - 1$ shows similarities across different collision systems, particularly for ε_3 . But even for ε_2 , the shape in Zr+Zr is similar to Au+Au just with an opposite sign.

Given the prevalent wiggly structures in $\rho_{\text{SHF}}/\rho_{\text{WS}}$ (Fig. 1b), we investigate the impact of the inner region ($r < R_0 - a$) and the surface region ($r > R_0 - a$) of $\rho(r)$. For this, we examine $R_O\{\text{mix}\} - 1$, which includes only the inner region's impact. These results, represented by open red symbols in Fig. 2 and compared across systems in Fig. 4, show small magnitudes ($\pm 0.5\%$) and are observable-dependent, but they exhibit the same N_{part} dependent shape across collision systems. The differences between $R_O\{\text{SHF}\} - 1$ and $R_O\{\text{mix}\} - 1$ (Fig. 2) represent the surface region's contribution, which clearly dominates the ε_3 ratio differences between SHF and WS.

We also consider whether the differences in ε_2 , ε_3 , or $p(N_{\text{part}})$ between SHF and WS can be absorbed by ad-

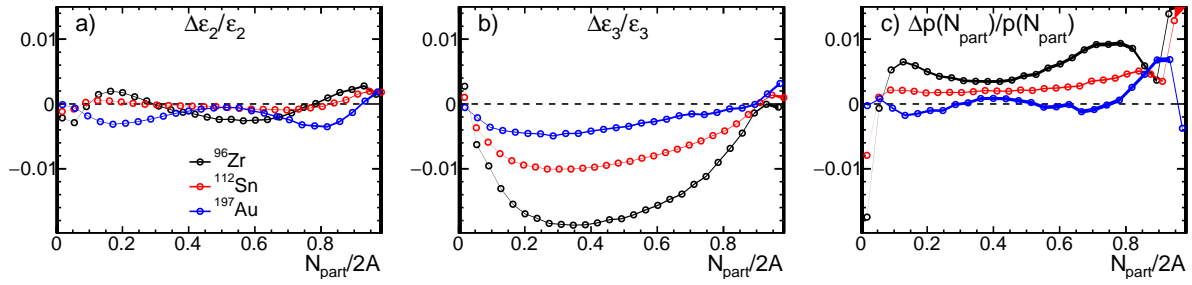


FIG. 3. Relative difference $R_{\mathcal{O}} - 1$ between SHF and WS with moment matching, where \mathcal{O} is ε_2 (left), ε_3 (middle), and $p(N_{\text{part}})$ (right) in Zr+Zr, Sn+Sn and Au+Au collisions. They are taken directly from Fig. 2.

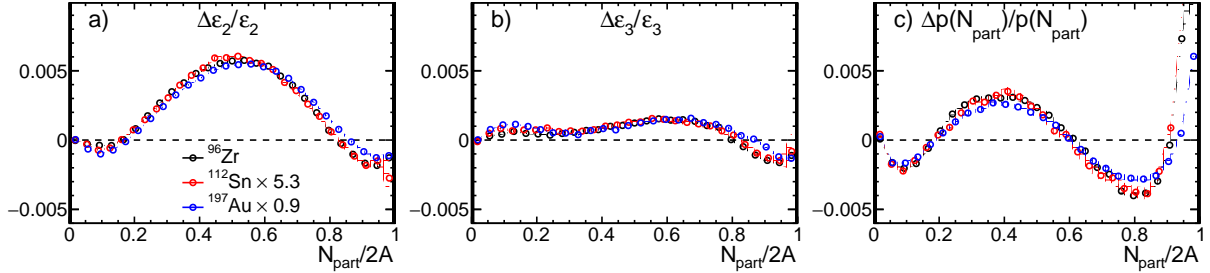


FIG. 4. Relative difference $R_{\mathcal{O}} - 1$ between ρ_{mix} and ρ_{pws} (i.e differing only in the inner region), where \mathcal{O} is ε_2 (left), ε_3 (middle), and $p(N_{\text{part}})$ (right) in Zr+Zr, Sn+Sn and Au+Au collisions. They are taken directly from Fig. 2.

justing the WS parameters R_0 and a alone:

$$\begin{aligned} R_{\mathcal{O}}\{\text{SHF}\} - 1 &= a_1(R_{\mathcal{O}}\{\text{WSa}^-\} - 1) + a_2(R_{\mathcal{O}}\{\text{WSR}^+\} - 1) \\ R_{\mathcal{O}}\{\text{mix}\} - 1 &= b_1(R_{\mathcal{O}}\{\text{WSa}^-\} - 1) + b_2(R_{\mathcal{O}}\{\text{WSR}^+\} - 1), \end{aligned} \quad (6)$$

where a and b are numerical coefficients common to all observables for a given collision species. We find that this adjustment can only be done for one observable at a time. For example, ε_2 in Fig. 4a can be adjusted by varying a , but this would induce a large reduction in ε_3 and an enhancement in $p(N_{\text{part}})$, which are not observed. Therefore, the influence of these fine structures on observables is real and can only be accurately studied via actual DFT calculations.

Overall, the impact of DFT's wiggly structures on observables is smaller than the expected variation in the skin parameter a in Zr+Zr and Ru+Ru isobar collisions but could be comparable to the variation induced by the radius parameter R_0 . Including wiggly structures in SHF induces changes that are about four times smaller for ε_2 (or 25%) and twice smaller for $p(N_{\text{part}})$ (or 50%) compared to a 0.06 fm variation in a . However, a comparable influence is observed for ε_3 . Thus, current WS parameterizations of DFT are sufficient for studying the structure impact on ε_2 and $p(N_{\text{part}})$ but not ε_3 [27].

Summary. We have demonstrated that the Woods-Saxon (WS) parameterization used to describe nucleon density distributions in heavy atomic nuclei fails to capture the detailed radial wiggle structure present in realistic Density Functional Theory (DFT) calculations. The differences between DFT (based on the Skyrme-

Hartree-Fock density functional) and WS parameterizations result in characteristic variations in observables for the initial state of heavy-ion collisions, such as ε_2 , ε_3 , and $p(N_{\text{part}})$. These differences, on a few percent level, are centrality- and observable-dependent, with similar shapes across different nuclei but distinct behaviors among the three observables. These variations cannot be simultaneously absorbed by merely re-adjusting the WS parameters.

The magnitude of the changes induced by the differences between SHF and WS is much smaller than the expected variations between isobar collisions, such as $^{96}\text{Ru}+^{96}\text{Ru}$ and $^{96}\text{Zr}+^{96}\text{Zr}$, a golden dataset for studying the impact of nuclear structure. However, these differences do limit the precision with which nuclear structure can be constrained using heavy-ion collisions based on WS parameterization. Therefore, actual DFT calculations should be used directly to gauge the systematic uncertainties.

Our work, together with earlier ones [8, 26], is the first step in quantifying whether the WS parameterization is sufficient in heavy-ion phenomenology. Future directions include considering the influence of nuclear deformation in DFT versus deformed WS parameterization [28], as well as studying other bulk observables such as mean transverse momentum fluctuations. More importantly, simulations based on state-of-the-art hydrodynamic models are required to quantify the impact of realistic DFT versus WS on the initial condition of QGP and the extraction of its transport properties. The un-

certainties in nuclear structure input should be included as part of the Bayesian analysis for heavy-ion collisions along the line of Ref. [29].

We thank G. Giacalone for useful comments. Z. Y and J.J are supported by DOE under Grants No. DE-SC0024602. JX is supported by the Strategic Priority Research Program of the Chinese Academy of Sciences under Grant No. XDB34030000, the NSFC under Grants No. 12375125, and the Fundamental Research Funds for the Central Universities.

APPENDIX

Figure 5a shows the nucleon density in the transverse (r_\perp, ϕ) plane, $\rho_\perp(r_\perp) = \int 2\pi r_\perp \rho dz dr_\perp$ for SHF. This distribution is directly used to calculate ε_n and N_{part} . Notably, in the interior region, the density of ^{96}Zr remains higher than that of ^{112}Sn , even after integration along the z-axis. The corresponding ratios between the SHF and WS distributions in the transverse plane are shown in Fig. 5b. Compared to Fig. 1b, the wiggle structures at $r_\perp \lesssim R_0$ are reduced but not eliminated, while the structures at $r_\perp \gtrsim R_0$ remain more or less unchanged.

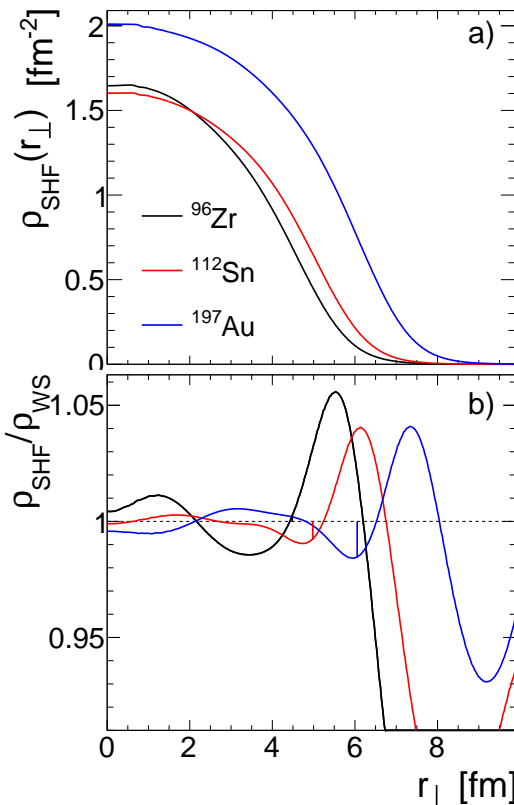


FIG. 5. (a) SHF nucleon density distributions in the transverse plane for ^{96}Zr , ^{112}Sn , and ^{197}Au nuclei. (b) Ratios of SHF and WS density distributions after moment matching and projection to the transverse plane. The vertical lines indicate the location $r_\perp = R_0 - a$.

*

†

‡

[1] U. Heinz and R. Snellings, *Ann. Rev. Nucl. Part. Sci.* **63**, 123 (2013), arXiv:1301.2826 [nucl-th].

[2] J.-Y. Ollitrault, *Eur. Phys. J. A* **59**, 236 (2023), arXiv:2308.11674 [nucl-ex].

[3] G. Giacalone, J. Jia, and V. Somà, *Phys. Rev. C* **104**, L041903 (2021), arXiv:2102.08158 [nucl-th].

[4] C. Zhang, S. Bhatta, and J. Jia, *Phys. Rev. C* **106**, L031901 (2022), arXiv:2206.01943 [nucl-th].

[5] STAR Collaboration, (2024), arXiv:2401.06625 [nucl-ex].

[6] H.-J. Xu, X. Wang, H. Li, J. Zhao, Z.-W. Lin, C. Shen, and F. Wang, *Phys. Rev. Lett.* **121**, 022301 (2018), arXiv:1710.03086 [nucl-th].

[7] G. Giacalone, J. Jia, and C. Zhang, *Phys. Rev. Lett.* **127**, 242301 (2021), arXiv:2105.01638 [nucl-th].

[8] H.-J. Xu, W. Zhao, H. Li, Y. Zhou, L.-W. Chen, and F. Wang, *Phys. Rev. C* **108**, L011902 (2023), arXiv:2111.14812 [nucl-th].

[9] G. Aad *et al.* (ATLAS), *Phys. Rev. C* **107**, 054910 (2023), arXiv:2205.00039 [nucl-ex].

[10] Q. Liu, S. Zhao, H.-J. Xu, and H. Song, *Phys. Rev. C* **109**, 034912 (2024), arXiv:2311.01747 [nucl-th].

[11] G. Giacalone *et al.*, (2024), arXiv:2402.05995 [nucl-th].

[12] P. Bożek and W. Broniowski, *Phys. Rev. C* **85**, 044910 (2012), arXiv:1203.1810 [nucl-th].

[13] H. Niemi, G. S. Denicol, H. Holopainen, and P. Huovinen, *Phys. Rev. C* **87**, 054901 (2013), arXiv:1212.1008 [nucl-th].

[14] J. Jia and C. Zhang, *Phys. Rev. C* **107**, L021901 (2023), arXiv:2111.15559 [nucl-th].

[15] M. Abdallah *et al.* (STAR), *Phys. Rev. C* **105**, 014901 (2022), arXiv:2109.00131 [nucl-ex].

[16] G. Nijs and W. van der Schee, *SciPost Phys.* **15**, 041 (2023), arXiv:2112.13771 [nucl-th].

[17] M. Bender, P.-H. Heenen, and P.-G. Reinhard, *Rev. Mod. Phys.* **75**, 121 (2003).

[18] H.-J. Xu, H. Li, X. Wang, C. Shen, and F. Wang, *Phys. Lett. B* **819**, 136453 (2021), arXiv:2103.05595 [nucl-th].

[19] L.-M. Liu, J. Xu, and G.-X. Peng, *Phys. Lett. B* **838**, 137701 (2023), arXiv:2301.07893 [nucl-th].

[20] M. Dutra, O. Lourenço, J. S. Sa Martins, A. Delfino, J. R. Stone, and P. D. Stevenson, *Phys. Rev. C* **85**, 035201 (2012), arXiv:1202.3902 [nucl-th].

[21] M. Dutra, O. Lourenço, S. S. Avancini, B. V. Carlson, A. Delfino, D. P. Menezes, C. Providência, S. Typel, and J. R. Stone, *Phys. Rev. C* **90**, 055203 (2014), arXiv:1405.3633 [nucl-th].

[22] L.-W. Chen, C. M. Ko, B.-A. Li, and J. Xu, *Phys. Rev. C* **82**, 024321 (2010), arXiv:1004.4672 [nucl-th].

[23] L.-M. Liu, C.-J. Zhang, J. Zhou, J. Xu, J. Jia, and G.-X. Peng, *Phys. Lett. B* **834**, 137441 (2022), arXiv:2203.09924 [nucl-th].

[24] M. L. Miller, K. Reygers, S. J. Sanders, and P. Steinberg, *Ann. Rev. Nucl. Part. Sci.* **57**, 205 (2007), arXiv:nucl-ex/0701025.

[25] J. Jia, G. Giacalone, and C. Zhang, *Phys. Rev. Lett.* **131**, 022301 (2023), arXiv:2206.10449 [nucl-th].

[26] Q. Y. Shou, Y. G. Ma, P. Sorensen, A. H. Tang, F. Videbæk, and H. Wang, *Phys. Lett. B* **749**, 215 (2015),

[arXiv:1409.8375](https://arxiv.org/abs/1409.8375) [nucl-th].

[27] However, the ε_3 seems not a good estimator for studying the nuclear structure impact on the v_3 in peripheral and mid-central region (see bottom panels of Fig. 2 in Ref. [14] and also [16]). Therefore it remains an open question whether considering WS parameters alone is ad-

equate for v_3 in peripheral and mid-central regions.

[28] W. Ryssens, G. Giacalone, B. Schenke, and C. Shen, *Phys. Rev. Lett.* **130**, 212302 (2023), [arXiv:2302.13617](https://arxiv.org/abs/2302.13617) [nucl-th].

[29] G. Giacalone, G. Nijs, and W. van der Schee, *Phys. Rev. Lett.* **131**, 202302 (2023), [arXiv:2305.00015](https://arxiv.org/abs/2305.00015) [nucl-th].